

# A topology optimization procedure for reinforced concrete structures

Oded Amir

Faculty of Civil and Environmental Engineering, Technion - Israel Institute of Technology

August 29, 2012

## 1 Abstract

A new topology optimization procedure for reinforced concrete structures is presented. The main application is reducing weight of concrete structures, which is highly desirable due to the negative environmental impact of cement production. The distribution of both concrete and reinforcement bars is optimized simultaneously. Concrete is modeled as a continuum exhibiting damage, into which reinforcement bars are embedded. Several examples demonstrate the capabilities of the procedure in generating efficient structures with a higher load-bearing capacity per unit weight, compared to standard designs. The proposed approach facilitates a fully digital work flow that can unify computer-based analysis, design and production.

Keywords: Reinforced concrete, Topology optimization, Sustainability, Continuum damage

## 2 Introduction

Computational procedures for structural optimization play an important role in improving product design in various industries. The automotive and aerospace industries, for example, make extensive use of such techniques for reducing weight and increasing stiffness, among other goals. In particular, topology optimization is emerging as a generic digital design tool that can be utilized in a wide range of engineering fields, spanning from nano-scale photonics up to furniture and airplanes [34]. So far, optimal design had little impact on traditional structural engineering as practiced in the construction industry. Considering the specific case of reinforced concrete design, optimization is exceptionally challenging because of the difficulty in combining numerical optimization tools with accurate constitutive models. Furthermore,

applying continuum topology optimization procedures is problematic because of the two distinct physical scales involved: reinforcement is achieved by inserting a very small volumetric ratio of discrete steel bars into the continuum concrete.

The drive towards sustainable structural design opens up great opportunities for applying optimization techniques in reinforced concrete design. Cement production is responsible for roughly 5% of man-made carbon dioxide emissions annually [39]. In fact, 900 kg of CO<sub>2</sub> are emitted for every 1000 kg of cement produced [26]. This motivates the search for design methodologies that facilitate weight reduction of concrete structures while maintaining the required load carrying capacity. The purpose of this article is to propose a computational optimization procedure aiming precisely at this goal.

Another motivating factor is the growing interest within the architectural community in topology optimization as a means of generating aesthetic and efficient structural forms [32, 13, 36]. Until recently, standard topology optimization procedures aimed at minimizing compliance of a linear-elastic structure were utilized for this purpose. This of course overlooks the true behavior of the construction material, especially in the case of concrete. Several studies that attempt to incorporate more realistic modeling have been published recently. Liu and Qiao [23] consider different stiffnesses of concrete and steel in order to generate layouts with distinct tension and compression members. Concrete-steel layouts were also discussed by Bogomolny and Amir [7] where elasto-plastic modeling and interpolated yield functions were used for representing the distinct stiffnesses and stress limits of the two materials. Similar results were later reported in [25] where stress constraints were imposed instead of modeling the complete nonlinear response. In a sense, the work by Victoria et al. [38] also deals with the challenge of generating two-material tension-compression layouts but there the focus is on generating strut-and-tie models rather than on structural forms. Despite providing an important step towards an applicable computational approach, the above mentioned procedures are still far from being usable. The main reasons are first, that the true behavior of concrete as a brittle strain-softening material is not considered; and second, that steel is modeled as a continuum occupying unrealistic volume ratios. The current study offers major improvements with respect to these two aspects.

Significant advancements in nonlinear finite element analysis of reinforced concrete structures facilitate the future development of computer-based automated design tools [16]. It is the purpose of this article to present a methodology that suggests a step forward towards digital design of reinforced concrete. The procedure enables to simultaneously optimize the distribution of both concrete and reinforcement by combining continuum- and truss-based topology optimization into a single problem formulation. In the nonlinear finite element analysis, we use a continuum damage model for concrete [30] together with the

embedded reinforcement formulation [31] that enables the representation of discrete reinforcement bars (rebars). As a framework we rely on the procedure suggested in [1] where the same modeling approach was taken but optimization was concerned only with the layout of reinforcement.

The focus of the current study is on the design of the so-called ‘D-regions’ in structural concrete where the strain distribution is nonlinear. In practice, strut-and-tie models are widely applied for positioning and quantifying the reinforcement in such regions of the structure [27, 33], but these of course assume a predefined shape of the concrete domain - while in our approach the distribution of concrete is not restricted to a certain shape and is a result of the optimization process. We note that as opposed to ‘D-regions’, in ‘B-regions’ such as beams, columns and frames, beam theory and cross-sectional analysis are sufficient for determining the necessary reinforcement. This means that applying structural optimization in the design of such elements may also be tackled by more simple approaches based on cross-sectional forces, especially if the shape of the cross-section is predefined and the aim is to optimize geometric sizes. This topic was addressed by numerous investigators since the 1970’s but is beyond the scope of this article. Clearly, achieving minimum weight of standard, repeated members such as beams, columns and slabs may offer a significant contribution to future practice. Based on the developments of the current study, the intention is to continue exploring the potential of combining nonlinear FE analysis with topology optimization procedures also for the design of beams, columns and slabs, in particular those that can be prefabricated.

The paper is organized as follows. First the finite element analysis is described in Section 3, with emphasis on the continuum damage model and on the embedded formulation in the context of truss topology optimization. Next we discuss the formulation of the optimization problem, parametrization of the design and adjoint sensitivity analysis in Section 4. Several examples of optimized reinforced concrete structures are presented Section 5. Finally, current results and future work are discussed in Section 6.

## **3 Finite element modeling**

### **3.1 Continuum damage model for concrete**

Plain concrete is assumed to behave as a strain-softening damaged continuum, according to the model suggested in [30]. This model was utilized successfully for optimization of fiber reinforced concrete [19, 18]. More recently, it was shown to be effective also for general reinforcement layout design [1]. The main principles of the constitutive model and its implementation in a finite element framework are

briefly presented in this section. We rely on the framework developed in [1] where a more detailed description of the model can be found.

Damage is assumed to be isotropic and therefore the process is defined by a single scalar variable  $D$ , where  $0 \leq D \leq 1$ . The stress-strain relation is given by

$$\boldsymbol{\sigma} = (1 - D)\mathbf{C} : \boldsymbol{\varepsilon} \quad (1)$$

where  $\boldsymbol{\sigma}$  is the stress tensor,  $\mathbf{C}$  is the elastic constitutive tensor and  $\boldsymbol{\varepsilon}$  is the strain tensor. The product  $\mathbf{C} : \boldsymbol{\varepsilon}$  is usually named the *effective stress* which acts on the actual resisting undamaged area (see for example [21] for an introduction to damage mechanics). The evolution of damage is governed by the history parameter  $\kappa$ . In the current study we utilize an exponential damage law [28]

$$D = 1 - \frac{\kappa_0}{\kappa} \left( 1 - \alpha + \alpha \exp^{-\beta(\kappa - \kappa_0)} \right)$$

where  $\kappa_0$  is a threshold value corresponding to the initiation of damage and  $\alpha$  and  $\beta$  are material constants. The history parameter corresponds to the extremal deformation of the material, measured in the multiaxial case by an equivalent strain. We adopt a simple equivalent strain measure that resembles the Drucker-Prager yield function [14]

$$\varepsilon_{eq} = \sqrt{3J_2} + mI_1$$

where  $J_2$  is the second invariant of the deviatoric strain;  $I_1$  is the trace of the strain tensor; and  $m$  is a material property that can be related to the ratio of strengths in uniaxial tension and compression. This equivalent strain measure is essentially used as a ‘damage detection surface’: once the equivalent strain at a certain material point exceeds the threshold value  $\kappa_0$ , damage begins to evolve at that point. The value of  $\kappa_0$  is set so that in uniaxial tension, damage will initiate when the cracking strain of concrete is exceeded. This means that for the particular case of uniaxial tension, the criterion  $\varepsilon_{eq} - \kappa_0 = 0$  is the same as the Rankine criterion.

An important feature of this particular damage model is the nonlocal formulation achieved by considering also spatial gradients of the equivalent strain. Thus typical difficulties in modeling of strain-softening materials are avoided, namely ill-posedness and mesh dependency (e.g. [3]). Assuming that the nonlocal equivalent strain denoted  $\bar{\varepsilon}_{eq}$  represents a weighted average of the local measure  $\varepsilon_{eq}$  over a

certain region, the following partial differential equation can be derived

$$\bar{\varepsilon}_{eq} - c\nabla^2\bar{\varepsilon}_{eq} = \varepsilon_{eq} \quad (2)$$

where  $c$  is of the dimension length squared in 2-D and length cubed in 3-D. We note that Eq. 2 is solved using a finite element discretization with the natural boundary conditions and can be conveniently coupled to the governing state equation of static equilibrium.

Applying the nonlocal approach,  $\kappa$  is determined at each material point according to the nonlocal equivalent strain  $\bar{\varepsilon}_{eq}$  through the Karush-Kuhn-Tucker conditions

$$\dot{\kappa} \geq 0, \quad \bar{\varepsilon}_{eq} - \kappa \leq 0, \quad \dot{\kappa}(\bar{\varepsilon}_{eq} - \kappa) = 0$$

meaning that a)  $\kappa$  never decreases; b)  $\kappa$  ‘registers’ the extremal nonlocal equivalent strain; and c) when  $\kappa$  grows, then necessarily  $\kappa = \bar{\varepsilon}_{eq}$ .

As in typical approaches to material nonlinearity, the evolution of damage is represented as a process evolving in ‘time’. Discretization of time is achieved by applying an incrementation scheme. For every time increment, the weak form of the partial differential equilibrium equation is discretized using finite elements, leading to the force balance equation

$$\mathbf{f}_{ext}^u - \mathbf{f}_{int}^u = \mathbf{0}$$

where  $\mathbf{f}_{ext}^u$  is the nodal external force vector accounting for volumetric, boundary and point loads. Similarly, the spatial discretization of Eq. (2) leads to

$$\mathbf{f}^e - \mathbf{K}^{\varepsilon\varepsilon}\bar{\varepsilon}_{eq} = \mathbf{0}$$

Then the typical iterative system of equations to be solved by the Newton-Raphson method, with iterative displacements and nonlocal equivalent strains as unknowns at cycle  $i$ , is expressed as

$$\begin{bmatrix} \mathbf{K}_{i-1}^{uu} & \mathbf{K}_{i-1}^{u\varepsilon} \\ \mathbf{K}_{i-1}^{\varepsilon u} & \mathbf{K}^{\varepsilon\varepsilon} \end{bmatrix} \begin{bmatrix} \delta\mathbf{u}_i \\ \delta\bar{\varepsilon}_{eq,i} \end{bmatrix} = \begin{bmatrix} \mathbf{f}_{ext}^u \\ \mathbf{f}_{i-1}^e \end{bmatrix} - \begin{bmatrix} \mathbf{f}_{int,i-1}^u \\ \mathbf{K}^{\varepsilon\varepsilon}\bar{\varepsilon}_{eq,i-1} \end{bmatrix} \quad (3)$$

where the incremental index is omitted for a clearer presentation. With the shape functions collected in  $\mathbf{N}$  and  $\tilde{\mathbf{N}}$  for the displacements and the nonlocal equivalent strains respectively (the shape functions

are not necessarily of the same order); and with their derivatives collected in  $\mathbf{B}$  and  $\tilde{\mathbf{B}}$  respectively, the components of Eq. (3) are

$$\begin{aligned}
\mathbf{K}_{i-1}^{uu} &= \int_{\Omega} \mathbf{B}^T (1 - D_{i-1}) \mathbf{C} \mathbf{B} d\Omega \\
\mathbf{K}_{i-1}^{u\epsilon} &= - \int_{\Omega} \mathbf{B}^T \mathbf{C} \epsilon_{i-1} q_{i-1} \tilde{\mathbf{N}} d\Omega \\
\mathbf{K}_{i-1}^{\epsilon u} &= - \int_{\Omega} \tilde{\mathbf{N}}^T \left( \frac{\partial \epsilon_{eq}}{\partial \epsilon} \right)_{i-1}^T \mathbf{B} d\Omega \\
\mathbf{K}^{\epsilon\epsilon} &= \int_{\Omega} (\tilde{\mathbf{N}}^T \tilde{\mathbf{N}} + \tilde{\mathbf{B}}^T c \tilde{\mathbf{B}}) d\Omega \\
\mathbf{f}_{int,i-1}^u &= \int_{\Omega} \mathbf{B}^T \sigma_{i-1} d\Omega \\
\mathbf{f}_{i-1}^{\epsilon} &= \int_{\Omega} \tilde{\mathbf{N}}^T \epsilon_{eq,i-1} d\Omega
\end{aligned}$$

Path-dependency enters the formulation through the scalar  $q$  which is non-zero only if  $\kappa$  (and therefore damage) is evolving with respect to the value at the previous converged increment denoted  $\kappa_{old}$

$$q_{i-1} = \begin{cases} \left( \frac{\partial D}{\partial \kappa} \right)_{i-1} & \text{if } \bar{\epsilon}_{eq,i-1} > \kappa_{old} \\ 0 & \text{if } \bar{\epsilon}_{eq,i-1} \leq \kappa_{old} \end{cases}$$

In practice, a displacement-controlled incrementation is more suitable due to the strain-softening response. This means that a prescribed iterative displacement, denoted  $\delta u^p$ , is enforced at a particular degree of freedom (DOF). Then we have an unknown iterative load factor  $\delta \theta$  instead of  $\delta u^p$  and the corresponding iterative equation system is slightly modified accordingly. In order to avoid modifying the tangent stiffness matrix (and for keeping its structure) we implement displacement control as suggested in [2].

### 3.2 Embedded reinforcement formulation

The main contribution of this study is in the simultaneous layout optimization of two material phases, concrete and steel reinforcement, that differ in geometrical scale as well as in mechanical behavior. Concrete occupies a continuum domain while steel rebars are essentially line components inserted into this domain before casting the concrete. Accordingly, in finite element procedures concrete is typically modeled by 2-D or 3-D continuum elements while rebars are represented by 1-D bar elements, having only axial stiffness. For optimizing the distribution of both phases within a single computational procedure, the so-called embedded formulation is employed. The embedded formulation was initially suggested in [31] and later extended in [12]. The main idea is that the stiffness of each individual rebar is added to

the stiffness of the surrounding concrete domain. In the current study, the bars are considered as linear elastic; nevertheless, considering elasto-plasticity does not affect the general applicability of the design approach.

Using the embedded formulation, the topological design problem consists of merging continuum-based and truss-based topology optimization approaches into a single design procedure. In continuum topology optimization, the design domain is typically discretized using a structured grid mesh with equilateral elements. In truss topology optimization, a so-called ‘ground structure’ is constructed such that it consists of all possible connectivities of bars within the design domain. These practices make the embedded formulation very attractive because the complete truss ground structure can be embedded into the continuum grid in a relatively simple manner. Moreover, practical design requirements can be automatically considered due to the flexibility in the generation of the truss ground structure. Examples are physical spacing between bars; clear concrete cover with no reinforcement near the edges of the domain; and orthogonal reinforcement patterns (without diagonal bars) which are easier to construct. Demonstrative examples for truss structures embedded into a structured grid in 2-D are presented in Figure 1.

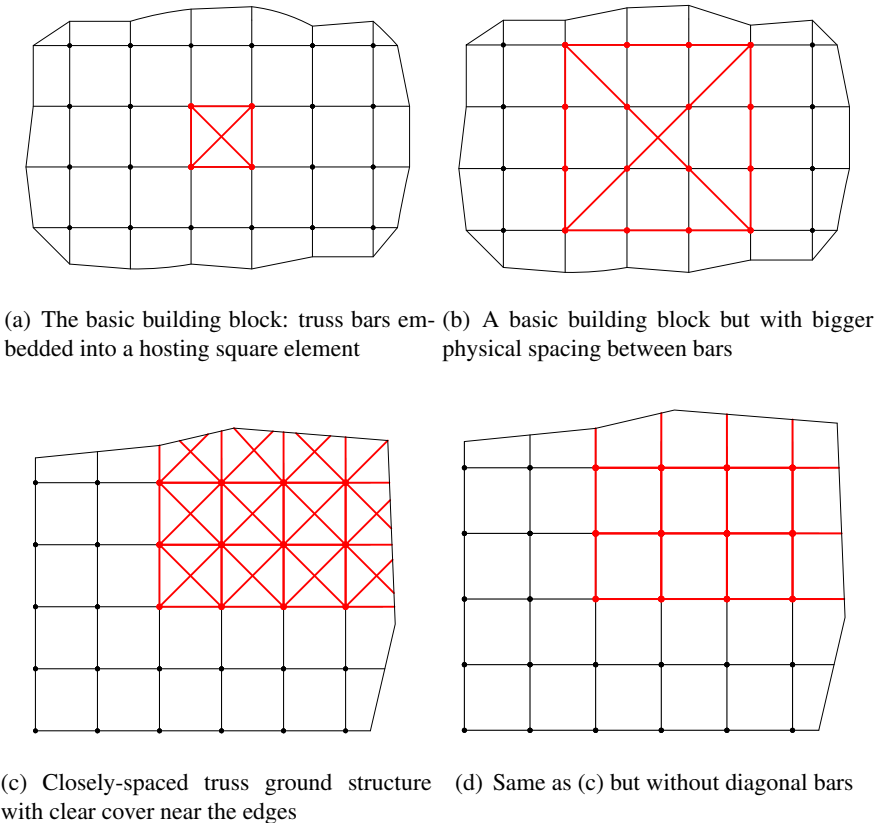


Figure 1: Demonstrative examples for truss structures embedded into a structured grid

The superposition of bar stiffnesses onto the hosting element stiffnesses is straightforward due to the way the ground structures are created. In essence, no element-level embedding is necessary because the truss elements share the same nodes as the hosting elements. This of course does not imply any loss of generality of the approach: the user may define bars in any location and embed them into the respective hosting elements. However, using a regularly-spaced truss structure with nodes that are compatible to those of the hosting mesh simplifies the embedding process by turning it into a global-level operation.

Finally, the contribution of the embedded truss structure to the global stiffness and internal force is added to the stiffness matrix and to the internal forces of the continuum domain. For a strain-softening response it is common to use displacement-controlled incrementation, meaning that the magnitude of a certain displacement is incrementally increased up to a prescribed value, as opposed to a gradual increase of the load. The typical iterative system (3) is modified to

$$\begin{bmatrix} \mathbf{K}_{i-1}^{uu} + \mathbf{K}^{bars} & \mathbf{K}_{i-1}^{u\varepsilon} \\ \mathbf{K}_{i-1}^{\varepsilon u} & \mathbf{K}^{\varepsilon\varepsilon} \end{bmatrix} \begin{bmatrix} \delta \mathbf{u}_i \\ \delta \bar{\varepsilon}_{eq,i} \end{bmatrix} = \begin{bmatrix} \delta \theta \hat{\mathbf{f}}_{ext}^u \\ \mathbf{f}_{i-1}^\varepsilon \end{bmatrix} - \begin{bmatrix} \mathbf{f}_{int,i-1}^u + \mathbf{f}_{int}^{bars} \\ \mathbf{K}^{\varepsilon\varepsilon} \bar{\varepsilon}_{eq,i-1} \end{bmatrix} \quad (4)$$

where  $\mathbf{K}^{bars}$  and  $\mathbf{f}_{int}^{bars}$  are the global stiffness matrix and internal forces corresponding to the complete set of truss bars;  $\delta \theta$  is an *unknown* iterative load factor and  $\hat{\mathbf{f}}_{ext}^u$  is a *fixed* reference load vector. One of the components in  $\delta \mathbf{u}$ , denoted  $\delta \mathbf{u}^p$ , is prescribed according to the chosen incrementation strategy. Solution of the system (4) can be obtained either by interchanging  $\delta \mathbf{u}^p$  with  $\delta \theta$  or by applying a specialized scheme [2] that maintains the pattern of the stiffness matrix. As above, incremental indices are omitted for clarity of the presentation.

## 4 Topology optimization

In this section, we present the formulation of the optimization problem and some details regarding the sensitivity analysis. In essence, we combine the classical density-based approach to continuum topology optimization [5, 4] together with the ground structure approach to truss topology optimization (see also [6] for an overview of both methods). The entities to be optimized are the spatial distribution of concrete and the cross-section areas of the steel bars. Distribution of concrete is represented by a density-like variable in each finite element, where a value of zero corresponds to void and a value of 1 corresponds to solid concrete. Each rebar segment is also represented by a design variable ranging from zero to 1, with the actual cross-section area given by a linear interpolation.

In the proposed design procedure, the goal of topology optimization is to minimize the volume of concrete subject to constraints on: 1) The load-bearing capacity of the structure; 2) The available volume of steel. Both concrete and steel rebars are freely distributed for achieving this aim. The nested approach to structural optimization is followed, meaning that the analysis is performed separately, leaving only the design variables inside the problem formulation

$$\begin{aligned}
\min_{\mathbf{x}} \phi(\mathbf{x}) &= \frac{\sum_{i=1}^{N_{elem}} \bar{x}_i}{N_{elem}} \\
\text{s.t.}: \quad g_1(\mathbf{x}) &= -\theta_{N_{in}} \hat{f}^p u_{N_{in}}^p + g^* \leq 0 \\
g_2(\mathbf{x}) &= \sum_{i=1}^{N_{bars}} a_i l_i - \rho V \leq 0 \\
0 \leq x_i &\leq 1, \quad i = 1, \dots, (N_{bars} + N_{elem}) \\
\text{with:} \quad \mathbf{R}_n(\mathbf{u}_n, \theta_n, \bar{\epsilon}_{eq,n}, \boldsymbol{\kappa}_{n-1}, \mathbf{x}) &= 0 \quad n = 1, \dots, N_{in} \\
\mathbf{H}_n(\bar{\epsilon}_{eq,n}, \boldsymbol{\kappa}_n, \boldsymbol{\kappa}_{n-1}) &= 0 \quad n = 1, \dots, N_{in} - 1
\end{aligned} \tag{5}$$

where  $N_{elem}$ ,  $N_{bars}$  and  $N_{in}$  are the number of continuum elements, the number of truss bars and the number of increments, respectively;  $\bar{\mathbf{x}}$  represents the physical distribution of concrete, related to the mathematical variables  $\mathbf{x}$  via filtering and projection operations;  $\mathbf{a}$  represents the physical cross-section areas of the truss bars, related to the mathematical variables  $\mathbf{x}$  via an interpolation function; the vector  $\mathbf{l}$  contains the bar lengths;  $g^*$  is a limit on the end-compliance of the structure;  $\rho$  is the volumetric ratio of reinforcement; and  $V$  is the volume of the design domain. We note that  $\phi$  is a simplified measure of the concrete volume fraction which is applicable when using a structured grid, where all elements have the same volume. This does not affect the generality of the formulation.

We choose to minimize volume subject to a constraint on compliance rather than vice-versa due to difficulties related to combining optimization with the damaged model. Comparing to standard minimum-compliance topology optimization procedures with linear-elastic materials, the consideration of damage introduces severe nonlinearity into the optimization problem. According to the author's experience, attempting to maximize the end-compliance subject to a volume constraint (the equivalent of compliance minimization in linear-elastic topology optimization) requires very conservative optimization strategies. This is because any change in the distribution of concrete leads to a corresponding change in the damage pattern. This results in 'zig-zag' updates of the design variables which can only be avoided by enforcing small step sizes on the update. Beginning with a full concrete domain eliminates this difficulty and leads to a much smoother optimization process. Furthermore, we use a continuation scheme where penalization and projection parameters are gradually increased. This also has a stabilizing effect

on the progress of the optimization.

In order to improve transparency in the presentation of the sensitivity analysis procedure, we artificially represent the structural analysis as a series of coupled equation systems corresponding to each of the ‘time’ increments. The first equation system is the global nonlinear incremental equilibrium that can be expressed as

$$\mathbf{R}_n(\mathbf{u}_n, \theta_n, \bar{\boldsymbol{\varepsilon}}_{eq,n}, \boldsymbol{\kappa}_{n-1}, \mathbf{x}) = \begin{bmatrix} \theta \hat{\mathbf{f}}_{ext}^u - (\mathbf{f}_{int}^u + \mathbf{f}_{int}^{bars}) \\ \mathbf{f}^e - \mathbf{K}^{e\varepsilon} \bar{\boldsymbol{\varepsilon}}_{eq} \end{bmatrix}_n = \mathbf{0}$$

where the unknowns at a certain increment  $n$  are the displacements  $\mathbf{u}_n$ , the load factor  $\theta_n$  and the nonlocal equivalent strains  $\bar{\boldsymbol{\varepsilon}}_{eq,n}$ ;  $\boldsymbol{\kappa}_{n-1}$  are the history parameters at the previous converged step, on a gauss point level; and  $\mathbf{x}$  is the vector of design variables. The second system is a collection of local equations which trace the path-dependencies throughout the evolution of damage

$$H_n(\bar{\boldsymbol{\varepsilon}}_{eq,n}, \boldsymbol{\kappa}_n, \boldsymbol{\kappa}_{n-1}) = 0$$

At each point, two possible states exist

$$H_n = \begin{cases} \boldsymbol{\kappa}_n - \bar{\boldsymbol{\varepsilon}}_{eq,n} & \text{if } \bar{\boldsymbol{\varepsilon}}_{eq,n} > \boldsymbol{\kappa}_{n-1} \\ \boldsymbol{\kappa}_n - \boldsymbol{\kappa}_{n-1} & \text{if } \bar{\boldsymbol{\varepsilon}}_{eq,n} \leq \boldsymbol{\kappa}_{n-1} \end{cases}$$

where we note that  $\bar{\boldsymbol{\varepsilon}}_{eq,n}$ ,  $\boldsymbol{\kappa}_n$  and  $\boldsymbol{\kappa}_{n-1}$  are Gauss point quantities. The relation to the nodal quantities used above is given by  $\bar{\boldsymbol{\varepsilon}}_{eq,n} = \tilde{\mathbf{N}} \bar{\boldsymbol{\varepsilon}}_{eq,n}^e$  where  $\bar{\boldsymbol{\varepsilon}}_{eq,n}^e$  are the nodal nonlocal equivalent strains in element  $e$ .

For obtaining an effective constraint on the end-compliance, a reasonable evaluation of  $g^*$  is required. For this purpose, we rely on results of a recent study, where truss topology optimization was utilized to distribute a given volume of steel reinforcement bars within a fixed concrete domain so that the stiffest structure is obtained [1]. The value of  $g^*$  represents a certain compromise with respect to the performance of the fixed concrete domain. For example,  $g^*$  can be set to 80% of the end-compliance of a full concrete structure with optimized reinforcement; then, a desirable result is that the minimum volume procedure generates a design using significantly less material than 80% of the design domain. We note that the compliance measure takes into account only the prescribed DOF (denoted by the superscript  $p$ ), but we apply concentrated loads that are distributed locally in the vicinity of the prescribed DOF so that a better finite element approximation is obtained.

## 4.1 Design parametrization

In the problem formulation (5), continuum- and truss-based topology optimization are combined into one unified procedure. The design variables  $\mathbf{x}$  correspond either to a continuum concrete element or to a steel rebar. For the finite element evaluation of the structural response, the design variables are transformed into physical quantities corresponding either to the ‘density’ of concrete or to the cross-section area of the steel bar. These are then used for computing the tangent stiffness and the internal forces.

For the concrete elements, first a standard density filter is applied [10, 8] with a simple linear weighting function to obtain  $\tilde{\mathbf{x}}$ . The purpose of applying a density filter is to overcome the well-known difficulty of artificial checkerboard patterns as well as to introduce a length scale in the design, thus avoiding results with very thin features that are difficult to manufacture. Then, a Heaviside projection function [17, 40] is utilized in order to ‘push’ the design towards a distinct 0-1 (or void-material) layout

$$\bar{x}_i = \begin{cases} \eta [e^{-\beta_{HS}(1-\tilde{x}_i/\eta)} - (1-\tilde{x}_i/\eta)e^{-\beta_{HS}}] & 0 \leq \tilde{x}_i \leq \eta \\ (1-\eta) [1 - e^{-\beta_{HS}(\tilde{x}_i-\eta)/(1-\eta)}] + \\ (\tilde{x}_i - \eta)/(1-\eta)e^{-\beta_{HS}} + \eta & \eta < \tilde{x}_i \leq 1 \end{cases} \quad (6)$$

where  $\eta$  is a threshold value and  $\beta_{HS}$  is a parameter determining the ‘sharpness’ of the smooth projection function. In the current study we use  $\eta = 0.5$ , meaning that any filtered density above 0.5 is projected to 1 and any value below 0.5 is projected to 0. The initial value of  $\beta_{HS}$  is set to either 0 or 1 and it is increased gradually as the optimization progresses. Heaviside projections are typically introduced in order to achieve crisp black-and-white layouts which are necessary in some design problems due to manufacturing requirements. This is not the case in concrete structures where a gradual reduction of thickness in the boundary of a hole is reasonable. Nevertheless, we use the projection with only mild values of  $\beta_{HS}$  (up to 4) in order to get clear topological layouts which can help understanding the load-carrying mechanism and the optimal placement of material.

At each material point represented by a finite element in the computational model, Young’s modulus of concrete is a function of the physical density following a modified SIMP rule [4, 35]

$$E(\bar{x}_i) = E_{min} + (E_{max} - E_{min})\bar{x}_i^{p_E} \quad (7)$$

where  $E_{min}$  is given a small positive value in order to avoid numerical difficulties;  $E_{max}$  is the actual value of Young’s modulus for concrete; and  $p_E$  is a penalization factor. In linear-elastic topology optimization procedures,  $p_E$  is typically set to 3. In the current implementation, we use a continuation scheme where

the penalty begins at 1 (linear interpolation) and is gradually increased to 3 so that distinct 0-1 designs are favorable. In principle, the interpolation (7) can accommodate also the case of distributing two materials (such as ‘soft’ and ‘stiff’ concrete) but this application is not within the scope of the current study. The dependence on density introduces a design dependence in the constitutive model (1) that now reads, for a certain element  $i$  and Gauss point  $gp$

$$\sigma_i^{gp} = (1 - D_i^{gp})E(\bar{x}_i)\mathbf{C}^0 \varepsilon_i^{gp} \quad (8)$$

where  $\mathbf{C}^0$  is a parametric constitutive tensor corresponding to  $E = 1$ . Note that matrix-vector notation is used here as opposed to tensor notation in (1).

As for the steel bars, the relation between the mathematical design variable and the corresponding area of bar  $i$  is given by a linear interpolation

$$a_i(x_i) = a_{min} + (a_{max} - a_{min})x_i$$

where  $a_i$  is the cross-section area;  $a_{min}$  and  $a_{max}$  are lower and upper bounds of the desired range of areas; and  $x_i$  is the design variable. The choice of  $a_{min}$  and  $a_{max}$  gives the user control over the outcome of optimization. For example,  $a_{min}$  may correspond to minimal reinforcement requirements. Another possibility is that  $a_{min}$  and  $a_{max}$  represent the range of bar types that are available for construction.

In principle, concrete and steel bars are distributed independently so it is possible to obtain an optimized layout where steel bars are ‘floating’ inside a void area which is not occupied by concrete. This of course is an undesirable result that can be avoided by penalizing (artificially reducing) the stiffness of such steel bars. This is performed in a manner similar to that of the standard density filter. Each bar is associated with a neighborhood of continuum elements. This includes all elements whose centroid lies within a certain distance from the bar’s centroid. Then the filtered design variable of the bar is given by

$$\tilde{x}_i = x_i \frac{1}{N_{ij}} \sum_{j \in N_i} (\bar{x}_j)^{pE} \quad (9)$$

where  $x_i$  is the mathematical variable corresponding to bar  $i$ ;  $N_i$  is the neighborhood of the bar;  $N_{ij}$  is the number of elements in the neighborhood;  $\bar{x}_j$  is the physical density of a concrete element  $j$  in the neighborhood; and  $\tilde{x}_i$  is the resulting filtered variable of the bar. In other words, within concrete regions of low density, the value of  $x_i$  is penalized in the same way as is the stiffness of the concrete. Then, the

stiffness matrix of the bar is given by the modified SIMP rule

$$\mathbf{K}_i = E_s (a_{min} + (a_{max} - a_{min}) \bar{x}_i^{p_{bar}}) \mathbf{K}_i^0$$

where  $E_s$  is Young's modulus of steel;  $p_{bar} \geq 1$  is a penalization factor and  $\mathbf{K}_i^0$  is a parametric stiffness matrix of the bar for  $E = 1$ ,  $a = 1$ . In principle, the most freedom is given to the optimization procedure when no penalization is considered ( $p_{bar} = 1$ ). The result in terms of continuously varying bar areas can then be post-processed to fit available bar types in practice. Nevertheless, one may consider adding penalization ( $p_{bar} > 1$ ) for various purposes. Examples are to approach a discrete design with a single bar type; or to obtain a 'clean' layout with realistic physical spacing between bars when the ground structure is relatively dense. For further discussion on this aspect the reader is referred to [1].

## 4.2 Sensitivity analysis

For using a first-order nonlinear programming method, we need to compute derivatives of the objective and of the general constraints with respect to changes in the design variables. The objective depends only on design variables attached to concrete elements. The sensitivity is given by the chain rule

$$\frac{\partial \phi(\mathbf{x})}{\partial x_i} = \frac{1}{N_{elem}} \frac{\partial \bar{x}_i}{\partial x_i} \frac{\partial \tilde{x}_i}{\partial x_i}$$

where the density filtering operation and (6) are differentiated to obtain the partial derivatives. Similarly, the reinforcement volume constraint  $g_2(\mathbf{x}) = \sum_{i=1}^{N_{bars}} a_i l_i - \rho V$  depends only on variables attached to rebars. It is differentiated to give

$$\frac{\partial g_2(\mathbf{x})}{\partial x_i} = (a_{max} - a_{min}) l_i$$

The constraint on the end-compliance  $g_1(\mathbf{x})$  involves also state variables so the sensitivities are computed by an adjoint procedure. The representation of the structural analysis as a transient coupled problem enables utilization of the framework by Michaleris et al. [29] which in our opinion leads to a rather transparent and convenient adjoint sensitivity analysis procedure. The procedure will be shortly presented in the following. For full details the reader is referred to [1] where the same functional was used as an objective. The constraint is expressed as a function of design and state variables, corresponding

only to the final temporal state denoted by  $N_{in}$

$$g_1(\mathbf{x}) = \bar{g}_1(\mathbf{u}_{N_{in}}(\mathbf{x}), \theta_{N_{in}}(\mathbf{x}), \bar{\epsilon}_{eq, N_{in}}(\mathbf{x}), \kappa_{N_{in}-1}(\mathbf{x}), \mathbf{x}) = -\theta_{N_{in}} \hat{f}^p u_{N_{in}}^p + g^*$$

We begin by writing the augmented functional

$$\begin{aligned} \hat{g}_1(\mathbf{x}) &= \bar{g}_1(\mathbf{u}_{N_{in}}(\mathbf{x}), \theta_{N_{in}}(\mathbf{x}), \bar{\epsilon}_{eq, N_{in}}(\mathbf{x}), \kappa_{N_{in}-1}(\mathbf{x}), \mathbf{x}) \\ &\quad - \sum_{n=1}^{N_{in}} \lambda_n^T \mathbf{R}_n(\mathbf{u}_n(\mathbf{x}), \theta_n(\mathbf{x}), \bar{\epsilon}_{eq, n}(\mathbf{x}), \kappa_{n-1}(\mathbf{x}), \mathbf{x}) \\ &\quad - \sum_{n=1}^{N_{in}-1} \sum_{gp=1}^{N_{gp}} \gamma_n H_n(\bar{\epsilon}_{eq, n}(\mathbf{x}), \kappa_n(\mathbf{x}), \kappa_{n-1}(\mathbf{x})) \end{aligned}$$

where  $\lambda_n$  and  $\gamma_n$  are incremental adjoint vectors in the global and local level respectively; and  $N_{gp}$  is the number of Gauss points in the finite element. The design sensitivities with respect to a certain variable  $x_i$  are then obtained from the explicit derivatives of the augmented functional

$$\frac{\partial g_1}{\partial x_i} = \frac{\partial \hat{g}_{1exp}}{\partial x_i} = \frac{\partial \bar{g}_1}{\partial x_i} - \sum_{n=1}^{N_{in}} \lambda_n^T \frac{\partial \mathbf{R}_n}{\partial x_i} = - \sum_{n=1}^{N_{in}} \lambda_n^T \frac{\partial \mathbf{R}_n}{\partial x_i} \quad (10)$$

The adjoint variables  $\lambda_n$  are determined by requiring that all implicit derivatives of the augmented functional are eliminated. This leads to a series of backwards-incremental linear systems of equations. The first system to be solved corresponds to the final increment  $N_{in}$

$$\tilde{\mathbf{K}}_{N_{in}}^T \lambda_{N_{in}} = \begin{pmatrix} - \left\{ \frac{\partial \bar{g}_1}{\partial \mathbf{u}_{N_{in}}^f} \right\}^T \\ \frac{\partial \bar{g}_1}{\partial \theta_{N_{in}}} \\ - \left\{ \frac{\partial \bar{g}_1}{\partial \bar{\epsilon}_{eq, N_{in}}} \right\}^T \end{pmatrix} = \begin{pmatrix} \mathbf{0} \\ -\hat{f}^p u_{N_{in}}^p \\ \mathbf{0} \end{pmatrix} \quad (11)$$

where the first part of the right-hand-side vector corresponds to free (non-prescribed) DOF, denoted by the superscript  $f$ ; the second part corresponds to the prescribed DOF, denoted by the superscript  $p$ ; and the third part corresponds to nonlocal equivalent strains DOF. The matrix  $\tilde{\mathbf{K}}_{N_{in}}$  is the same as  $\mathbf{K}_{N_{in}}$  except for a modification of the column denoted by the superscript  $p$  corresponding to the prescribed DOF

$$\begin{aligned} \tilde{\mathbf{K}}_{N_{in}}^f &= \mathbf{K}_{N_{in}}^f \\ \tilde{\mathbf{K}}_{N_{in}}^p &= \frac{\partial \mathbf{R}_{N_{in}}}{\partial \theta_{N_{in}}} \end{aligned}$$

Stepping backwards to increment  $N_{in} - 1$ , we aim to eliminate the implicit derivatives  $\frac{\partial \kappa_{N_{in}-1}}{\partial \mathbf{x}}$ . This

is achieved by setting the local adjoint variables

$$\gamma_{N_{in}-1} = \frac{\partial \bar{g}_1}{\partial \kappa_{N_{in}-1}} - \left\{ \frac{\partial \mathbf{R}_{N_{in}}}{\partial \kappa_{N_{in}-1}} \right\}^T \quad \lambda_{N_{in}} = - \left\{ \frac{\partial \mathbf{R}_{N_{in}}}{\partial \kappa_{N_{in}-1}} \right\}^T \lambda_{N_{in}}$$

where the equality  $\frac{\partial H_{N_{in}-1}}{\partial \kappa_{N_{in}-1}} = 1$  was utilized. The derivative  $\frac{\partial \mathbf{R}_{N_{in}}}{\partial \kappa_{N_{in}-1}}$  is non-zero only in points where path-dependency occurs at increment  $N_{in}$ , meaning damage was determined by  $\kappa_{N_{in}-1}$  rather than by  $\bar{\epsilon}_{eq,N_{in}}$ . From here a general form for the global adjoint equation that holds for increments  $n = 1, \dots, N_{in} - 1$  is revealed. It is the same as Eq. (11) but has no derivatives of  $\bar{g}_1$  and has an additional right-hand-side term involving  $\gamma_n$  which introduces the path-dependency. This additional term is an assembly onto the global level of local terms corresponding to points where  $\frac{\partial H_n}{\partial \bar{\epsilon}_{eq,n}}$  is non-zero. Then the linear system to be solved in the general increment is

$$\tilde{\mathbf{K}}_n^T \lambda_n = \begin{Bmatrix} \mathbf{0} \\ 0 \\ \left\{ \tilde{\mathbf{N}}^T \frac{\partial H_n}{\partial \bar{\epsilon}_{eq,n}} \gamma_n \right\} \end{Bmatrix} \quad (12)$$

Finally, the general form for the expression used to compute the local adjoints, that holds for increments  $n = 1, \dots, N_{in} - 2$  is revealed as

$$\gamma_n = - \left\{ \frac{\partial \mathbf{R}_{n+1}}{\partial \kappa_n} \right\}^T \lambda_{n+1} - \frac{\partial H_{n+1}}{\partial \kappa_n} \gamma_{n+1} \quad (13)$$

During the process of stepping back in ‘time’, the incremental contributions to the sensitivity (10) are collected. For reinforcement bars we have  $\frac{\partial \mathbf{R}_n}{\partial x_i} = - \frac{\partial (\mathbf{f}_{int}^{bars})_n}{\partial x_i}$ . This involves the derivative of the internal forces with respect to the filtered variable, multiplied by the differentiation of the filtering operation (9), yielding

$$\frac{\partial \mathbf{R}_n}{\partial x_i} = - \frac{\partial (\mathbf{f}_{int}^{bars})_n}{\partial \tilde{x}_i} \frac{\partial \tilde{x}_i}{\partial x_i} = \left( -p_{bar} \tilde{x}_i^{(p_{bar}-1)} (a_{max} - a_{min}) E_s \mathbf{K}_i^0 \mathbf{u}_{n,i} \right) \frac{1}{N_{ij}} \sum_{j \in N_i} (\tilde{x}_j)^{pE}$$

where  $\mathbf{u}_{n,i}$  are the displacements computed at increment  $n$  in the  $i$ -th bar’s degrees of freedom; and the index  $j$  represents concrete elements within the neighborhood of the bar  $i$ . For concrete elements we have  $\frac{\partial \mathbf{R}_n}{\partial x_i} = - \frac{\partial (\mathbf{f}_{int}^u + \mathbf{f}_{int}^{bars})_n}{\partial x_i}$  because concrete densities contribute not only to concrete forces but also to bar forces via the filtering of the bar variables (9). Applying the chain rule gives

$$\frac{\partial \mathbf{R}_n}{\partial x_i} = - \left( \frac{\partial (\mathbf{f}_{int}^u)_n}{\partial \tilde{x}_i} + \frac{\partial (\mathbf{f}_{int}^{bars})_n}{\partial \tilde{x}_j} \frac{\partial \tilde{x}_j}{\partial \tilde{x}_i} \right) \frac{\partial \tilde{x}_i}{\partial \tilde{x}_i} \frac{\partial \tilde{x}_i}{\partial x_i}$$

where the index  $i$  represents a certain concrete element; the index  $j$  represents a certain bar which has the element  $i$  within its neighborhood; and the following expressions are used

$$\begin{aligned}\frac{\partial (\mathbf{f}_{int})_n}{\partial \bar{x}_i} &= \sum_{gp=1}^{N_{gp}} w \mathbf{J} \mathbf{B}^T \frac{\partial \sigma_i^{gp}}{\partial \bar{x}_i} \\ \frac{\partial \sigma_i^{gp}}{\partial \bar{x}_i} &= (1 - D_i^{gp}) \mathbf{C}^0 \varepsilon_i^{gp} (E_{max} - E_{min}) p_E \bar{x}_i^{p_E - 1} \\ \frac{\partial \bar{x}_j}{\partial \bar{x}_i} &= x_j \frac{1}{N_{ji}} p_E \bar{x}_i^{p_E - 1}\end{aligned}$$

For clarification,  $w$  and  $J$  are the weight and the determinant of the Jacobian corresponding to the Gauss point; and  $N_{ji}$  is the number of concrete elements present in the neighborhood of bar  $j$  (notice the swap of indices with respect to the original formula).

Concluding this section, we note that the computed design sensitivities were found to be in perfect agreement with numerical derivatives based on finite differences.

## 5 Examples

Several examples of optimized reinforced concrete designs are presented in this section. In the current study, the proposed procedure is applied to the design of load-bearing structures that qualify as ‘D-regions’, where self-weight is insignificant with comparison to the external load. The loads are in principle point forces which are distributed locally in order to avoid artificial stress concentrations due to the finite element discretization. A small prescribed displacement is imposed at the central loading point and the analysis is performed using displacement control with adaptive incrementation. In the examples presented, the number of increments was usually between 6 to 10 and the number of Newton-Raphson iterations per increment between 1 to 5. In all examples, the continuum mesh for concrete consists of square, 4-node bi-linear plane stress elements. Material properties are kept constant for all examples as presented in Table 1. The de-localization parameter  $c$  in Eq. (2) is set according to the particular geometry. The procedure is implemented in FORTRAN and the optimization is performed by the Method of Moving Asymptotes - MMA [37].

Table 1: Material properties used in all examples

$E_{min}$ [MPa]	$E_{max}$ [MPa]	$\nu$	$\kappa_0$	$m$	$\alpha$	$\beta$	$E_s$ [MPa]
300	30,000	0.2	$1.818 \times 10^{-4}$	0.818	0.95	100	200,000

An important aspect of the implementation is the continuation scheme. The penalization parameters  $p_E$  and  $p_{bar}$ , as well as the Heaviside projection parameter  $\beta_{HS}$ , are gradually increased as described

in Table 2. Applying strong penalization and sharp projection from the beginning of the optimization process may aggravate difficulties due to the highly nonlinear and non-convex nature of the problem. This is avoided by the gradual continuation. As a consequence, a fixed number of iterations is performed instead of enforcing a strict convergence tolerance.

Table 2: Implemented continuation schemes

Iterations	Deep beam			Corbel			Wall		
	$p_E$	$p_{bar}$	$\beta_{HS}$	$p_E$	$p_{bar}$	$\beta_{HS}$	$p_E$	$p_{bar}$	$\beta_{HS}$
1-100	1.00	1.00	1.00	1.00	1.00	0.00	1.00	1.00	0.00
101-200	2.00	1.05	2.00	2.00	1.00	0.00	2.00	1.00	0.00
201-300	3.00	1.10	4.00	3.00	1.00	1.00	3.00	1.00	1.00
301-400				3.00	1.05	2.00	3.00	1.05	2.00
401-500				3.00	1.10	4.00	3.00	1.10	4.00

In the current implementation, the truss ground structures consist of bars in 0 and 90 degrees; in some cases we allow diagonal (45 degrees) bars as well. The purpose is to reflect the practical preference for such layouts, but this might pose a certain limitation as the flow of forces is affected by the direction of the bars. We note that the design approach is general and can accommodate any bar pattern. It is expected that by allowing more diverse bar directions, performance can be improved even further; this effect will be examined in future work.

As will be seen in the following examples, steel rebars are positioned primarily in tensile regions where concrete is damaged. In some cases, rebars are also used for stiffening compressive regions. This is expected because the solution of (5) represents a trade-off between concrete volume and load-bearing capacity. Positioning stiff rebars in compression enables the reduction of concrete volume while satisfying the compliance constraint. In case the designer wishes to avoid reinforcement in compression, the problem formulation can be modified accordingly, for example by: 1) Minimizing also the steel volume; or 2) Considering an artificial material model for steel where compression is penalized.

## 5.1 Deep beam

As a first example we consider the design of a deep beam. The problem setting and the computational model for analysis and optimization are presented in Figure 2. Our main result refers to a ground structure consisting of 5,580 elements and 2,250 bars, meaning a total of 7,830 design variables. The truss ground structure consists of horizontal, vertical and diagonal bars arranged regularly with a spacing of 9 finite elements (roughly 0.1m) between adjacent horizontal and vertical bars. The values of  $a_{min}$  and  $a_{max}$  are set to zero and  $4.0 \times 10^{-3}$ [m<sup>2</sup>/m] respectively and  $c = 4.2 \times 10^{-3}$ [m<sup>2</sup>]. The constraint on compliance denoted as  $g^*$  in the problem formulation (5) is set to  $2.8 \times 10^{-2}$ [kNm], which is roughly 80% of the

load-bearing capacity of the full concrete beam with optimized reinforcement as reported in [1]. The available volume of steel is 0.5% of the volume of the design domain; the prescribed displacement is 0.5[mm] and the filter radius is 0.035[m].

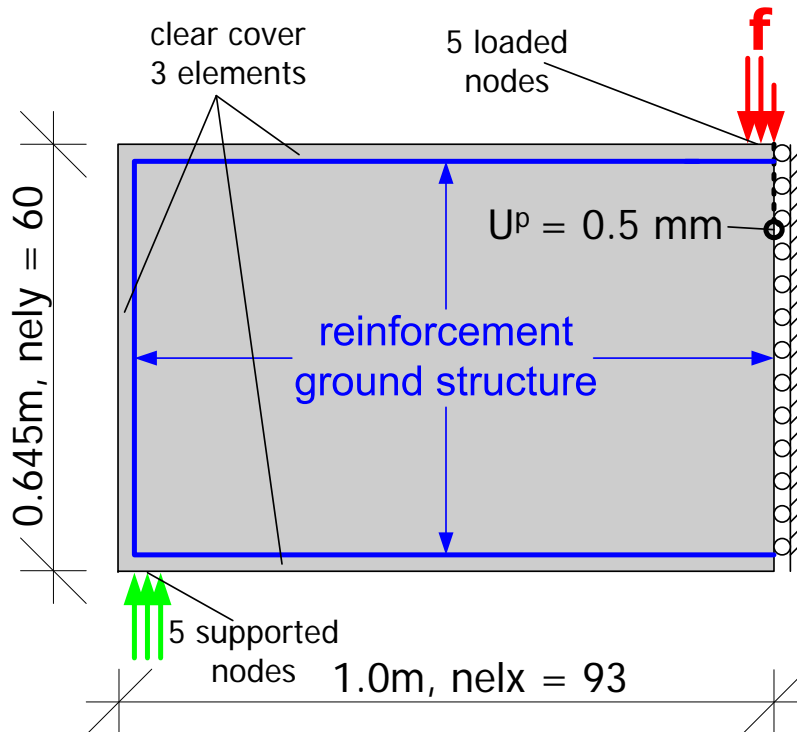


Figure 2: Problem setting and computational model, symmetric half of a 2-D deep beam

The evolution of the objective function and the layouts obtained at every step of the continuation scheme are presented in Figure 3. It can be seen that concrete is gradually cut out of unnecessary regions and new holes are created. At the same time, most of the steel is positioned in the bottom fiber in order to resist the tensile forces. A small portion of steel is also positioned in the vicinity of the concentrated load due to its higher stiffness that is clearly preferable for enhancing the load-bearing capacity. The resulting structure can bear 80% of the load that can be carried by a full concrete beam, but its weight is only 65.6% of the weight of the full beam. This means that per unit weight, we achieve 22% more load-bearing capacity compared to the standard full beam. This demonstrates the potential of utilizing optimization procedures to reduce material consumption while ensuring a viable design.

The same example problem was examined with a reinforcement ground structure that does not contain diagonal rebars. This is typically preferable due to easier construction. The resulting distribution of concrete is practically identical in both cases, and the only difference is in the absence of rebars under the loaded region. Essentially, the optimization procedure could not fit rebars effectively into the diagonal concrete member so no reinforcement was positioned in this region. As compensation, the minimized

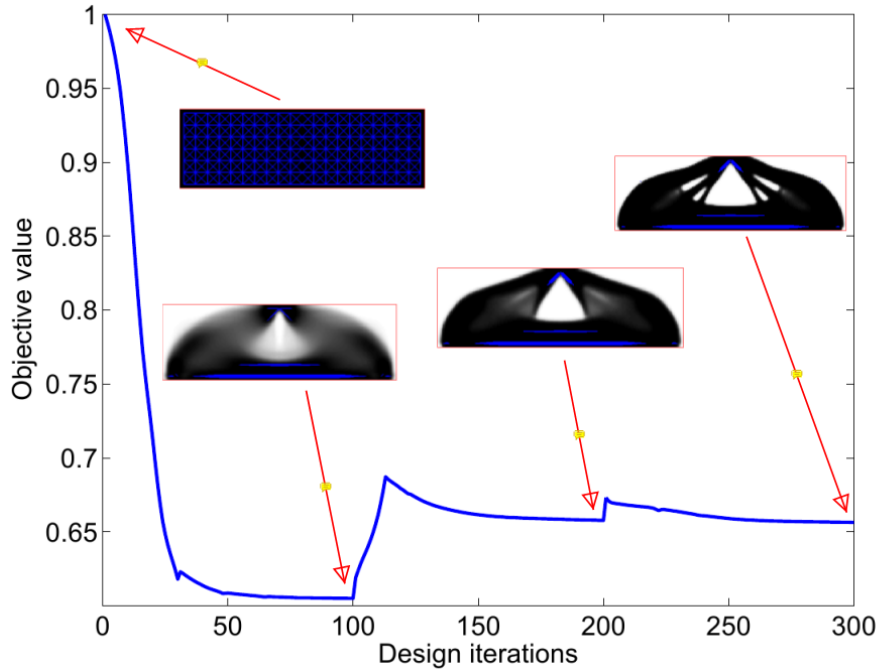
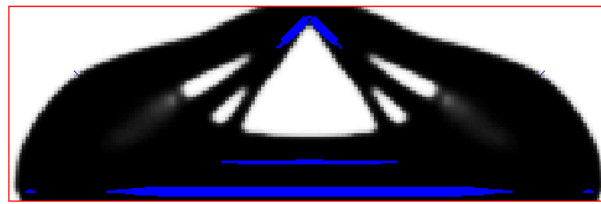


Figure 3: Topology optimization of a deep beam: convergence of the objective and snapshots of the optimized layouts. The final design occupies 65.6% of the whole design domain but can bear 80% of the load carried by the whole beam.

volume achieved was 66.0% compared to 65.6% with the diagonal rebars available. Both layouts are presented for comparison in Figure 4.

Looking towards practical application of optimization in structural design, an important observation is that a conventional linear-elastic topology optimization procedure yields a design that is inferior in performance compared to the design obtained with the damage-based procedure. For investigating this aspect, we first performed a standard minimum compliance topology optimization with a volume constraint corresponding to our proposed design, i.e. a volume fraction of 65.6%. Then we embedded the optimized reinforcement layout and ran 100 design iterations (with the parameters of stage 3 in Table 2), to allow for redistribution of both concrete and steel. The starting and final layouts are presented in Figure 5. The result is that with the starting design, the compliance constraint is violated; and with the final design, the constraint is fulfilled but the concrete volume fraction is raised to 69.8%. This means that employing a more elaborate material model is worthwhile, despite the cost in heavier computation. Furthermore, this comparison clarifies that the applicability of optimization procedures based on linear-elastic modeling is limited when considering design with other materials that exhibit nonlinear phenomena such as damage, fracture or plasticity.

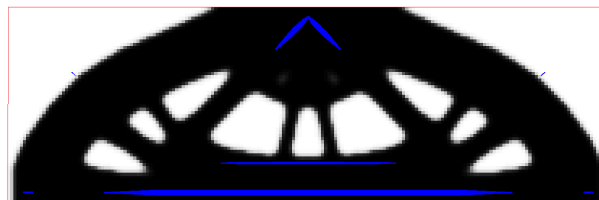


(a) Ground structure includes diagonals,  $\phi = 0.6564$

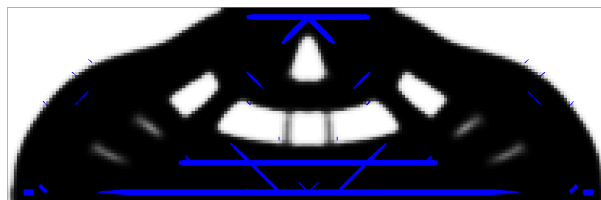


(b) Ground structure without diagonals,  $\phi = 0.6601$

Figure 4: Topology optimization of a deep beam: final layouts and objective values with two different reinforcement ground structures.



(a) First iteration:  $\phi = 0.6564$  but compliance constraint is violated



(b) After 100 iterations:  $\phi = 0.6980$  and constraints fulfilled

Figure 5: Topology optimization of a deep beam with an initial design obtained from a linear-elastic procedure: performance is inferior compared to the proposed damage-based procedure.

## 5.2 Corbel

In this example we consider the design of a 2-D corbel, which was previously examined by several researchers in the context of applying continuum topology optimization for generating strut-and-tie models [22, 20, 9, 38]. The setting of the problem is given in Figure 6. The ground structure consists of 6,372 elements and 3,606 bars, meaning a total of 9,978 design variables. The truss ground structure consists of horizontal, vertical and diagonal bars arranged regularly with a spacing of 6 finite elements (0.1m) between adjacent horizontal and vertical bars. The values of  $a_{min}$  and  $a_{max}$  are set to zero and  $4.9 \times 10^{-3}[\text{m}^2/\text{m}]$  respectively and  $c = 4.4 \times 10^{-3}[\text{m}^2]$ . The constraint on compliance is set to  $6.0 \times 10^{-2}[\text{kNm}]$ , corresponding to 80% of the load-bearing capacity of the full concrete corbel with optimized reinforcement [1]. The available volume of steel is 0.5% of the volume of the design domain; the prescribed displacement is 0.5[mm] and the filter radius is 0.05[m].

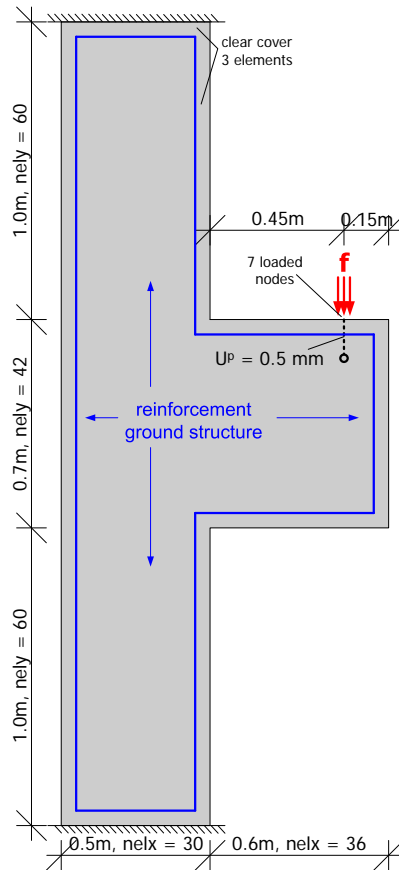


Figure 6: Problem setting and computational model, 2-D corbel

The evolution of the objective function and the layouts obtained at every step of the continuation scheme are presented in Figure 7. Steel rebars are mainly positioned in the vicinity of the reentrant corner where the highest tensile stresses appear. Additionally, a few rebars are positioned near the perimeter of

the corbel and act in compression. Again, the optimized design offers significant reduction in material consumption. The ratio of load-bearing capacity to weight is improved by nearly 32% compared to the standard full concrete domain.

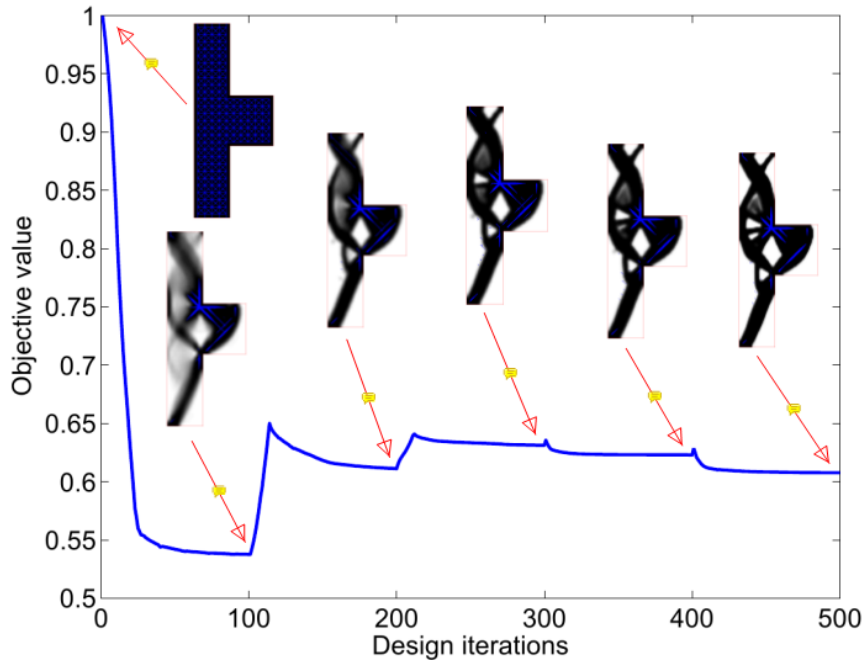


Figure 7: Topology optimization of a corbel: convergence of the objective and snapshots of the optimized layouts. The final design occupies 60.8% of the whole design domain but can bear 80% of the load carried by the whole corbel.

In principal, the optimized layout resembles the results obtained in the studies mentioned above that focused on using topology optimization for generating strut-and-tie models. However, the current approach cannot be directly compared to such procedures because it yields a final design that does not occupy the complete domain; while in the strut-and-tie modeling approach the actual sizing of members (as well as the choice of material for tensile members) is performed in a post-processing stage. In most studies [22, 20, 9], it was proposed to use layouts generated by linear elastic minimum-compliance procedures as strut-and-tie models. Once the model is determined, the designer needs to decide which material (concrete or steel) to use for the members undergoing tension and to size all members, according to the magnitude of the forces. As an exception, in [38] different stiffnesses for steel and concrete were considered when generating the optimized layout but the result still needs to be post-processed: the sizing of members does not consider stress limits and steel is modeled as a continuum rather than by discrete bars.

In this study, we do not attempt to generate strut-and-tie models. The main goal is to cut out unnecessary concrete, and naturally we obtain layouts that look like strut-and-tie models; but the choice

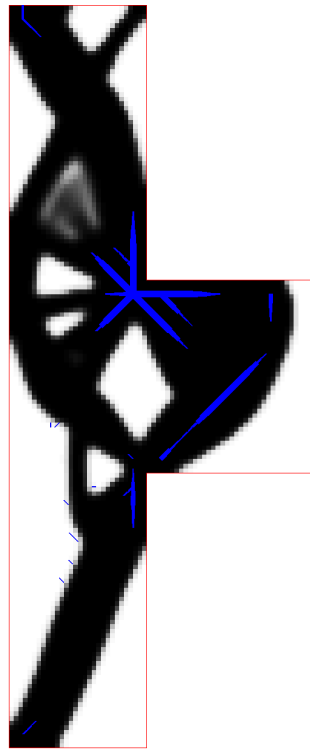
of material as well as the sizing are performed automatically. This is due to the more realistic approach taken based on: a) The consideration of damage; and b) The embedding of reinforcement bars. Consequently, concrete members in the optimized layout are sized according to their true stress state, whether it is dominated by tension or by compression. Moreover, ‘ties’ to be designed in steel can only be given a standard shape (defined by the ground structure) whereas in most previous studies they were freely positioned due to the continuum modeling. Another important result obtained with the proposed procedure is the utilization of concrete in tension. This is demonstrated on the corbel example, see Figure 8. In the optimized layout, some of the tensile members are made of plain concrete which is utilized up to the allowable tensile stress. Such resolution cannot be captured by optimization procedures based on linear elasticity.

### 5.3 Wall with opening

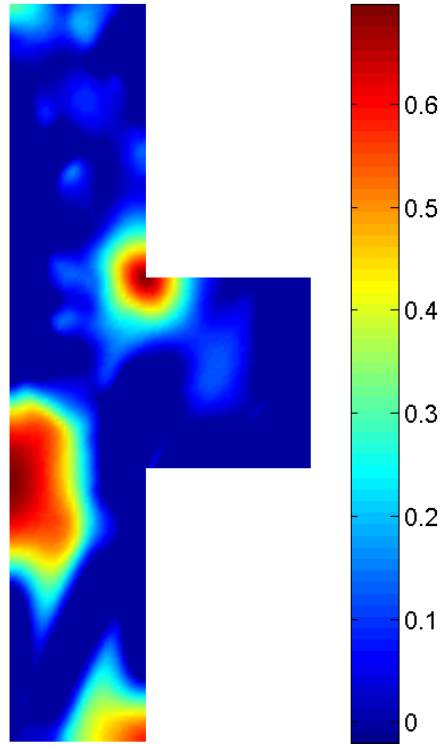
In this example we aim at optimizing the design of a wall with an opening, see Figure 9 for the problem setting. Schlaich et al. [33] gave it thorough consideration when demonstrating the strut-and-tie modeling approach for design of structural concrete. It was also used as an example for applying continuum topology optimization as a means of generating strut-and-tie models [22, 20, 9, 38]. The ground structure consists of 13,200 elements and 2,780 bars, meaning a total of 15,980 design variables. The truss ground structure consists of horizontal and vertical bars arranged with varying spacing between adjacent bars, see the first snapshot in Figure 10. The values of  $a_{min}$  and  $a_{max}$  are set to zero and  $8.01 \times 10^{-3}[\text{m}^2/\text{m}]$  respectively and  $c = 9.8 \times 10^{-2}[\text{m}^2]$ . The constraint on compliance is set to  $1.5[\text{kNm}]$ , which is slightly higher than the load-bearing capacity of the initial design - a full concrete domain with evenly distributed reinforcement (meaning the first few iterations are infeasible). The available volume of steel is 0.5% of the volume of the design domain; the prescribed displacement is  $2.5[\text{mm}]$  and the filter radius is  $0.3[\text{m}]$ .

The evolution of the objective function and the layouts obtained at every step of the continuation scheme are presented in Figure 10. The load is transferred to the right-hand-side support via a thick concrete block; and to the left-hand-side support via a system of tension and compression members. Reinforcement bars are mainly used in the bottom fiber and to reduce damage around the window. Some reinforcement is also added above the right-hand-side support that bears most of the load. As with the corbel, the optimized layout is in principle similar to a strut-and-tie model but offers a detailed design that accounts for the tensile capacity of concrete.

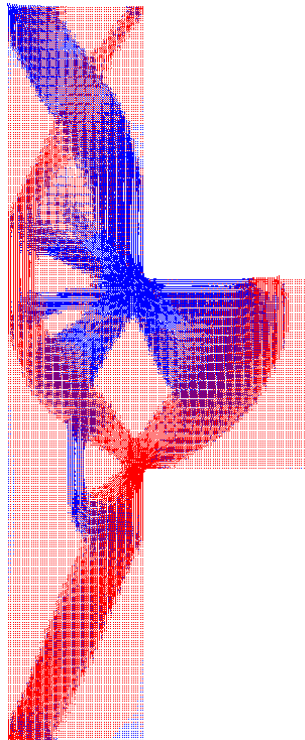
We now turn to demonstrate the effect of the filter (9) that is applied in order to avoid uncovered steel rebars in the optimized layout. The optimized design of the wall is compared to that obtained without



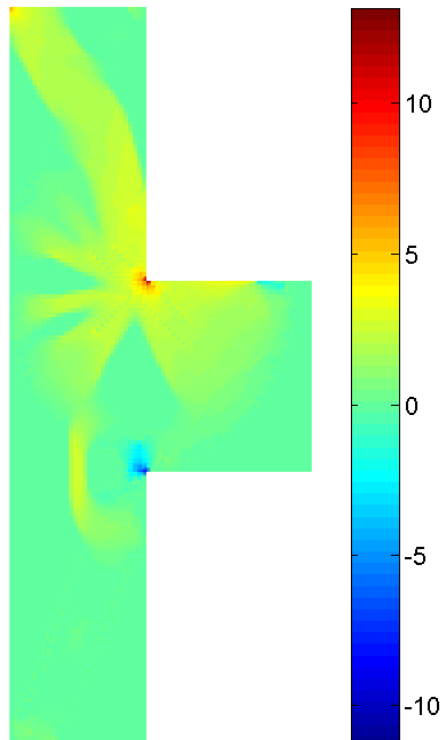
(a) Optimized layout,  $\phi = 0.6077$



(b) Damage in the optimized layout



(c) Principal stresses in the optimized layout



(d) Maximum principal stress  $\sigma_1$  in the optimized layout

Figure 8: Topology optimization of a corbel: for achieving maximum stiffness, concrete is utilized in tension up to its allowable tensile stress (3 MPa). This causes slight damage in plain concrete regions.

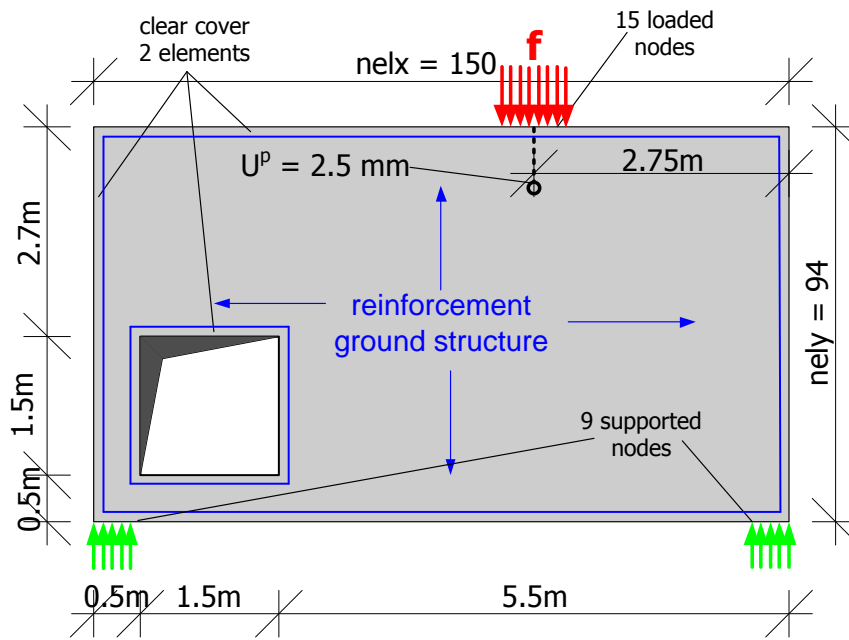


Figure 9: Problem setting and computational model, 2-D wall with opening

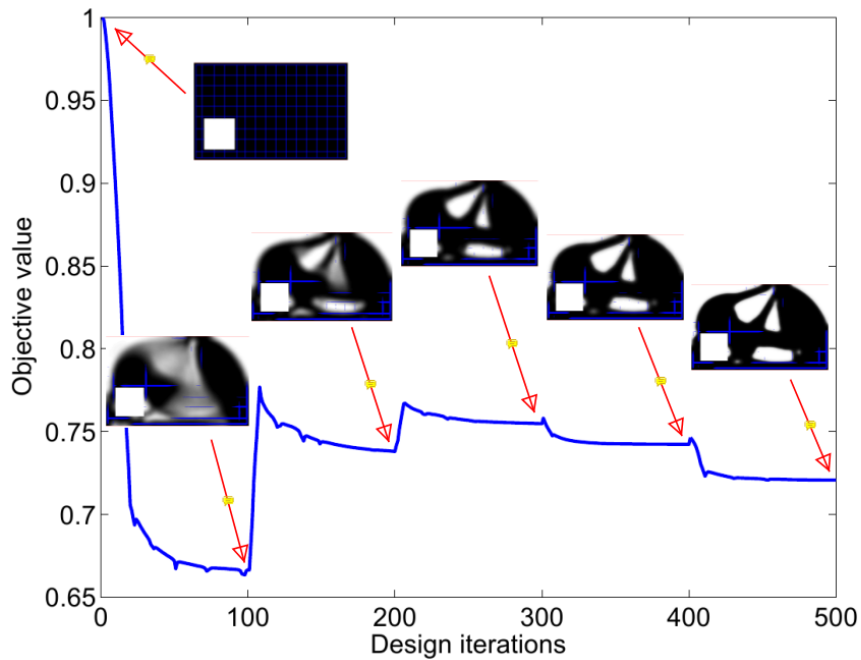
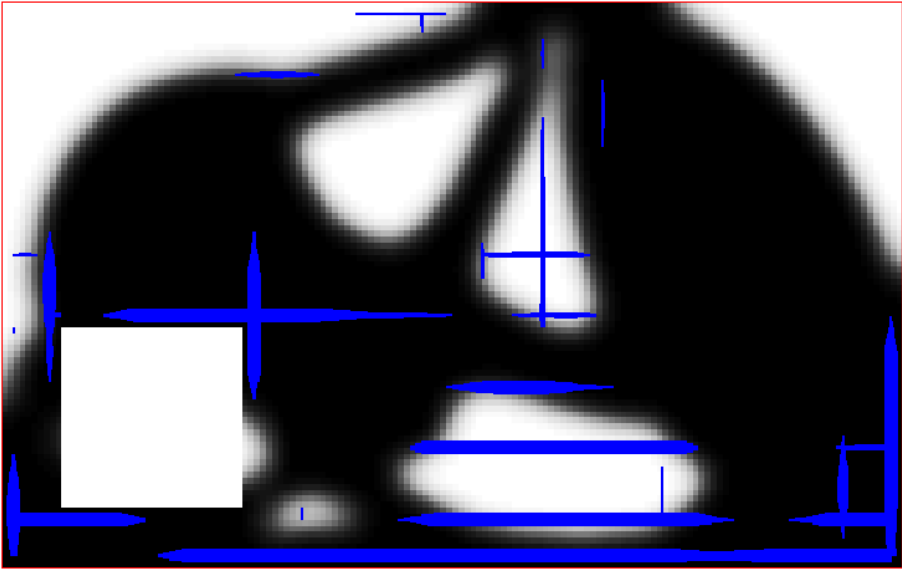
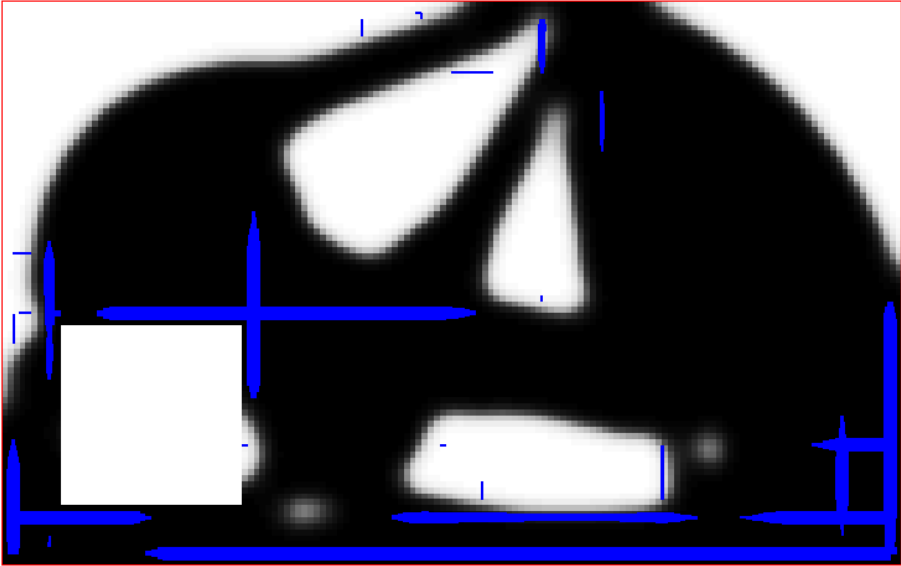


Figure 10: Topology optimization of a wall with an opening: convergence of the objective and snapshots of the optimized layouts. The final design occupies 72.1% of the whole design domain but can bear more than the load carried by the whole wall with evenly distributed reinforcement.

such filter in Figure 11. When no filter on bar areas is applied, we obtain ‘floating’ rebars that are not properly covered by concrete. From a pure optimization point of view, this yields a superior objective because these bars are used as stiffeners of holes, thus facilitating further reduction in the volume of concrete. However, from a practical point of view such a result is undesirable and it can be seen that by applying the filter, most of the isolated rebars are eliminated. It is possible that slightly higher penalty values are necessary for completely eliminating all isolated bars.



(a) No filter applied on bar variables: steel bars are used to strengthen the holes yielding a better objective,  $\phi = 0.7084$



(b) Bar variables are filtered according to the neighboring concrete densities: no exposed rebars and a higher objective,  $\phi = 0.7207$

Figure 11: Topology optimization of a wall with an opening: the effect of applying a filter to ensure rebars are covered by concrete.

## 6 Discussion

A new computational procedure for optimizing reinforced concrete structures was presented. The main idea is to combine realistic finite element modeling of reinforced concrete with topology optimization procedures based on a completely consistent sensitivity analysis. Concrete is modeled as a continuum where strain-softening response is considered by means of a nonlocal damage model. Reinforcement is represented by a set of all acceptable positions of rebars and is embedded into the continuum concrete domain. Both phases, concrete and reinforcement, are designed simultaneously in a topology optimization procedure combining truss-based and continuum-based methods.

The main goal is to achieve a reduction in the weight of concrete structures. This is motivated by the need to reduce cement production which is a major source of CO<sub>2</sub> emissions. Facilitating the design of lighter concrete structures can therefore be seen as a crucial step towards sustainable design. With respect to the load-bearing capacity per unit weight, it was shown that the optimized designs perform 20% to 30% better than standard structures. Furthermore, several examples demonstrate the benefits of utilizing a relatively elaborate material model that requires a path-dependent nonlinear analysis and a corresponding sensitivity analysis. The resulting designs outperform those obtained by standard procedures based on linear elasticity, due to the consideration of the true material properties. In this study we only considered weight and load-bearing capacity as the objective and constraint. Nevertheless, the methodology is general and other quantities such as cost or extent of cracking can be introduced based on proper modeling.

As of today, the main application of topology optimization in reinforced concrete design is in generating strut-and-tie models. While the references mentioned throughout the text focus on generating the strut-and-tie model which then needs to be solved for dimensioning, in the current approach several design steps are performed within a single computational procedure: distribution of both concrete and steel is optimized and the necessary sizes of members are found. This suggests much bigger potential for topology optimization in reinforced concrete design.

At this point it is difficult to compare the optimized designs to the state of the art reflected in building codes. Some design requirements can be easily included, e.g. clear concrete cover and minimum reinforcement, but some post-processing is still required in order to satisfy typical building codes. Furthermore, current codes are based primarily on strut-and-tie modeling, assuming a fully cracked concrete domain at the ultimate limit state; while we perform a nonlinear FE analysis and apply only small deformations for initiating damage. The main assumption in developing the current design procedure is that in

future practice, nonlinear FE analysis will be widely accepted as a means of predicting the true response. This will facilitate design procedures that are based on optimization and may enable the consideration of more realistic behavior, for example accounting for the contribution of concrete in tension. In the near future we intend to incorporate more advanced constitutive models for the concrete phase, which combine plasticity with either damage (e.g. [24, 15]) or fracture (e.g. [11]). By considering a more realistic prediction of the concrete's response, we believe that this approach can be applied to both serviceability as well as ultimate limit states. Another important goal of future work is extending the formulation to deal with structures carrying their own self weight (particularly slabs), where we expect the reduction in weight to be even more significant.

An attractive aspect of the suggested procedure is the fully digital work flow. Using CAD software, a detailed truss ground structure can be easily defined and exported to the finite element software. Automatic embedding of the truss elements is then performed, a rather straightforward operation especially if only structured grids are used. Once the optimized topology of both concrete and rebars is found, it can be exported back to the CAD system and then used for producing concrete molds by innovative methods, e.g. fabric-formed; CNC milling; or CNC hotwire foam cutting. Such a computational design tool can be very effective especially for designing complex 2-D and 3-D concrete structures.

## 7 Acknowledgements

This work was funded by the Danish Council for Independent Research | Technology and Production Sciences, during the author's employment as a postdoctoral researcher at the Department of Mechanical Engineering, Technical University of Denmark. This support is gratefully acknowledged. The author wishes to thank the anonymous reviewers for their helpful comments; and also thanks Krister Svanberg for the FORTRAN MMA code.

## References

- [1] O. Amir and O. Sigmund. Reinforcement layout design for concrete structures based on continuum damage and truss topology optimization. *Structural and Multidisciplinary Optimization*, 2012. In press.
- [2] J.-L. Batoz and G. Dhatt. Incremental displacement algorithms for nonlinear problems. *International Journal for Numerical Methods in Engineering*, 14:1262–1267, 1979.

- [3] Z. P. Bažant, T. B. Belytschko, and T. Chang. Continuum theory for strain-softening. *ASCE Journal of Engineering Mechanics*, 110(12):1666–1692, 1984.
- [4] M. P. Bendsøe. Optimal shape design as a material distribution problem. *Structural Optimization*, 1:193–202, 1989.
- [5] M. P. Bendsøe and N. Kikuchi. Generating optimal topologies in structural design using a homogenization method. *Computer Methods in Applied Mechanics and Engineering*, 71:197–224, 1988.
- [6] M. P. Bendsøe and O. Sigmund. *Topology Optimization - Theory, Methods and Applications*. Springer, Berlin, 2003.
- [7] M. Bogomonly and O. Amir. Conceptual design of reinforced concrete structures using topology optimization with elasto-plastic material modeling. *International Journal for Numerical Methods in Engineering*, 2012. Published online.
- [8] B. Bourdin. Filters in topology optimization. *International Journal for Numerical Methods in Engineering*, 50:2143–2158, 2001.
- [9] M. Bruggi. Generating strut-and-tie patterns for reinforced concrete structures using topology optimization. *Computers and Structures*, 87(23-24):1483–1495, 2009.
- [10] T. E. Bruns and D. A. Tortorelli. Topology optimization of non-linear elastic structures and compliant mechanisms. *Computer Methods in Applied Mechanics and Engineering*, 190:3443–3459, 2001.
- [11] J. Červenka and V. K. Papanikolaou. Three dimensional combined fracture-plastic material model for concrete. *International Journal of Plasticity*, 24(12):2192 – 2220, 2008.
- [12] T. Chang, H. Taniguchi, and W. Chen. Nonlinear finite element analysis of reinforced concrete panels. *ASCE Journal of Structural Engineering*, 113:122–140, 1987.
- [13] P. Dombernowsky and A. Søndergaard. Three-dimensional topology optimisation in architectural and structural design of concrete structures. In *Proceedings of the International Association for Shell and Spatial Structures (IASS) Symposium*, Valencia, Spain, 2009.
- [14] D. C. Drucker and W. Prager. Soil mechanics and plastic analysis or limit design. *Quarterly of Applied Mathematics*, 10(2):157–165, 1952.

- [15] P. H. Feenstra and R. de Borst. A composite plasticity model for concrete. *International Journal of Solids and Structures*, 33:707–730, 1996.
- [16] fib Task Group 4.4. *Practitioners’ guide to finite element modelling of reinforced concrete structures*. International Federation for Structural Concrete (fib), Lausanne, Switzerland, 2008.
- [17] J. K. Guest, J. H. Prévost, and T. Belytschko. Achieving minimum length scale in topology optimization using nodal design variables and projection functions. *International Journal for Numerical Methods in Engineering*, 61:238–254, 2004.
- [18] J. Kato and E. Ramm. Optimization of fiber geometry for fiber reinforced composites considering damage. *Finite Elements in Analysis and Design*, 46(5):401–415, 2010.
- [19] J. Kato, A. Lipka, and E. Ramm. Multiphase material optimization for fiber reinforced composites with strain softening. *Structural and Multidisciplinary Optimization*, 39(1):63–81, 2009.
- [20] H.-G. Kwak and S.-H. Noh. Determination of strut-and-tie models using evolutionary structural optimization. *Engineering Structures*, 28(10):1440–1449, 2006.
- [21] J. Lemaître and R. Desmorat. *Engineering Damage Mechanics*. Springer, Berlin Heidelberg, 2005.
- [22] Q. Liang, Y. Xie, and G. Steven. Topology optimization of strut-and-tie models in reinforced concrete structures using an evolutionary procedure. *ACI Structural journal*, 97(2):322–330, 2000.
- [23] S. Liu and H. Qiao. Topology optimization of continuum structures with different tensile and compressive properties in bridge layout design. *Structural and Multidisciplinary Optimization*, 43: 369–380, 2011. doi: 10.1007/s00158-010-0567-x.
- [24] J. Lubliner, J. Oliver, S. Oller, and E. Oñate. A plastic-damage model for concrete. *International Journal of Solids and Structures*, 25:299–326, 1989.
- [25] Y. Luo and Z. Kang. Layout design of reinforced concrete structures using two-material topology optimization with druckerprager yield constraints. *Structural and Multidisciplinary Optimization*, 2012. doi: 10.1007/s00158-012-0809-1. Published online.
- [26] N. Mahasenan, S. Smith, and K. Humphreys. The cement industry and global climate change: Current and potential future cement industry CO<sub>2</sub> emissions. In J. Gale and Y. Kaya, editors, *Greenhouse Gas Control Technologies - 6th International Conference*, pages 995 – 1000. Pergamon, Oxford, 2003. doi: 10.1016/B978-008044276-1/50157-4.

- [27] P. Marti. Truss models in detailing. *Concrete International*, 7:66–73, 1985.
- [28] J. Mazars and G. Pijaudier-Cabot. Continuum damage theory - application to concrete. *ASCE Journal of Engineering Mechanics*, 115(2):345–365, 1989.
- [29] P. Michaleris, D. A. Tortorelli, and C. A. Vidal. Tangent operators and design sensitivity formulations for transient non-linear coupled problems with applications to elastoplasticity. *International Journal for Numerical Methods in Engineering*, 37:2471–2499, 1994.
- [30] R. H. J. Peerlings, R. de Borst, W. A. M. Brekelmans, and J. H. P. de Vree. Gradient enhanced damage for quasi-brittle materials. *International Journal for Numerical Methods in Engineering*, 39(19):3391–3403, 1996.
- [31] D. Phillips and O. Zienkiewicz. Finite element nonlinear analysis of concrete structures. *ICE proceedings*, 61(1):59–88, 1976.
- [32] M. Sasaki. *Morphogenesis of Flux Structure*. Architectural Association Publications, London, 2007.
- [33] J. Schlaich, K. Schafer, and M. Jennewein. Toward a consistent design of structural concrete. *PCI journal*, 32(3):74–150, 1987.
- [34] O. Sigmund and M. P. Bendsøe. Topology optimization: from airplanes to nano-optics. In K. Stubbkjær and T. Kortenbach, editors, *Bridging from technology to society*. Technical University of Denmark, Lyngby, Denmark, 2004.
- [35] O. Sigmund and S. Torquato. Design of materials with extreme thermal expansion using a three-phase topology optimization method. *Journal of the Mechanics and Physics of Solids*, 45(6):1037–1067, 1997.
- [36] L. L. Stromberg, A. Beghini, W. F. Baker, and G. H. Paulino. Application of layout and topology optimization using pattern gradation for the conceptual design of buildings. *Structural and Multidisciplinary Optimization*, 43:165–180, 2011.
- [37] K. Svanberg. The method of moving asymptotes - a new method for structural optimization. *International Journal for Numerical Methods in Engineering*, 24:359–373, 1987.

- [38] M. Victoria, O. M. Querin, and P. Martí. Generation of strut-and-tie models by topology optimization using different material properties in tension and compression. *Structural and Multidisciplinary Optimization*, 44:247–258, 2011.
- [39] World Business Council for Sustainable Development. The cement sustainability initiative: executive brief. Technical report, 2012.
- [40] S. Xu, Y. Cai, and G. Cheng. Volume preserving nonlinear density filter based on heaviside functions. *Structural and Multidisciplinary Optimization*, 41(4):495–505, 2010. doi: 10.1007/s00158-009-0452-7.